

Photoproduction of J/ψ with forward hadron tagging in hadronic collisions

TICHOUK,¹ HAO SUN,^{1,*} and XUAN LUO¹

¹*Institute of Theoretical Physics, School of Physics, Dalian University of Technology,
No.2 Linggong Road, Dalian, Liaoning, 116024, P.R.China*

(Dated: April 19, 2022)

We study the photoproduction of J/ψ using the NRQCD formalism with forward hadron tagging at the Large Hadron Collider. We estimate the total cross sections and event rates with and without nuclear shadowing effects in high energy proton-proton, proton-nucleus and nucleus-nucleus collisions. Our results show that the processes which involve J/ψ photoproduction depend on the choice of forward detector acceptances ξ . Under some precise cut of $p_T^{J/\psi}$ and $z^{J/\psi}$ kinematic variables, we find that the distributions of photoproduction of J/ψ are led by the Fock state $^1S_0^{[8]}$ or $^3S_1^{[1]}$. The total cross sections and event rates will be smaller if the nuclear shadowing effects are considered. The processes give a crucial photoproduction signature at the LHC with forward detector acceptances. The exploration and the detection of the interactions will be useful for studying the mechanism of heavy quarkonium production.

I. INTRODUCTION

Since the discovery of heavy quarkonia in the mid-1970s, their production and decay become reliable tools to improve our understanding of theoretical aspects of quantum chromodynamics (QCD) from the hard region, where the strong interaction is realized with a large momentum transfer, to the soft region, where the strong interaction is carried out with a small momentum transfer. These production and decay of heavy quarkonia are studied under the non-relativistic quantum chromodynamics (NRQCD) due to the large mass of heavy quarks ($m_c \sim 1.5$ GeV, $m_b \sim 4.75$ GeV). The full description of the theoretical framework was proposed by Bodwin, Braaten and Lepage(BBL) [1]. It factorizes the quarkonium production in terms of short distance QCD cross sections and long distance matrix elements (LDMEs). The former can be perturbatively evaluated in series of the running coupling constant α_s while the latter is the probability for a heavy $Q\bar{Q}$ pair with spin S , orbital angular momentum L , total angular momentum J , and color multiplicity $a = 1$ (color-singlet), 8 (color-octet) to evolve into a physical heavy quarkonium state. The value of LDMEs can either be calculated by utilizing non-perturbative methods or extracted phenomenologically from data [2], i.e., QCD lattice simulations or measurements in some production processes. The $Q\bar{Q}$ pair is generated from the partonic interaction at short distances in color singlet (CS) or in color-octet (CO) states and hadronizes into physical CS observable by emitting soft gluons non-perturbatively. The effect of LDME contribution has a hierarchically ordered scaling with v [3], v being the nonrelativistic velocity of Q or \bar{Q} in the $Q\bar{Q}$ rest frame. The essence of this theory can now be systematically shortened by the double expansion in powers of α_s and v . A lot of phenomenological approaches of this framework are meticulously narrated in Refs [4, 5, 7, 8], taking into account the complete and spanned structure of the $Q\bar{Q}$ Fock space by the state $n = ^{2S+1}L_J^{(a)}$.

However, the golden age of the NRQCD theory has been to address the limitations of the early proposed models from which it establishes its coherently solid postulations. The most notable mechanisms for quarkonium production are the color-singlet model (CSM), color octet mechanism (COM), color-evaporation model (CEM) and fragmentation-function approach (FFA). In the CSM [9–23], the spin and the color quantum numbers of $Q\bar{Q}$ pair don't change during the hadronization due to the absence of gluon emission, it is restricted by sorting out the infrared divergences in P-wave and D-wave decay widths of heavy quarkonium, and it is also incapable to handle the high transverse momentum spectrum of J/ψ in experiments. However, the spin and the color quantum numbers of $Q\bar{Q}$ pair do change during the hadronization with the emission of gluons [24] in COM. The CEM depends more on statistical factors and is unable to explain the ratio of the P_T distribution of J/ψ and χ_{CJ} , both in photo- and hadroproduction from experiments [25–28]. In the FFA [29, 30], the cross section can be written in terms of convolution of the partonic production cross section with light-cone fragmentation functions at large transverse momentum.

More recently, the accessibility of experimental data including the feed-down and non-prompt contributions has provided a very good description of J/ψ photoproduction in a wide energy range [24, 31, 32] in investigating color-singlet and color-octet contributions. Though there are many studies of J/ψ production within NRQCD factorization

*Electronic address: haosun@mail.ustc.edu.cn haosun@dlut.edu.cn

approach have been carried out in, for example, γN [33], γp [34], e^+e^- [35], forward rapidity pp [36], $p\bar{p}$ and ep [37] collisions, the theoretical tools for the explanation of decay and production quarkonium at existing colliders are still under intense debate. For that reason, we should predict paths to examine more heavy quarkonium production and decay for the future colliders.

A plan [38] which is suggested by the FP420 R&D Collaboration in 2009 allows to study forward physics at the LHC such as the study pomeron-induced processes, low-x QCD physics, hadronic models of ultra high energy cosmic rays and photon-photon interactions, etc [39]. To reach this new realm of interest, detectors in the LHC tunnel need to be readjusted so as to precisely measure very forward hadrons. The setting-up of forward detectors at LHC may permit to predict the single diffraction and double pomeron exchange cross sections [40] which are important for future measurements at the LHC, may endow the likelihood to open a new window to investigate new physics even up to TeV scale [41–44] with extremely clean environment, and may enable to tag forward hadron or nucleus in photon-hadron and photon-nucleus collisions at high rapidity regions. It may also offer knowledge about unexplored phase space areas. The acceptance of the forward hadron detector system is defined as the region of the interaction and dependent on the mass of the centrally produced system. The interval of collision is classified as follows: $0.1 < \xi_1 < 0.5$, $0.0015 < \xi_2 < 0.5$ for CMS-TOTEM forward detector, and $0.015 < \xi_3 < 0.15$ for AFP-ATLAS forward detector [38]. The probe of coherent interactions in existing and future colliders with the installation of additional detectors at low scattering angle and with the outgoing particle remaining intact after collision is feasible [45].

In this present work, we estimate the predictions of the cross sections of single J/ψ photoproduction for the coherent processes in proton-proton, proton-nucleus, nucleus-nucleus interactions including both $2 \rightarrow 1$ and $2 \rightarrow 2$ subprocesses. The illustrative diagram of J/ψ meson photoproduction by photon induced process at LHC is shown in Fig.1. A

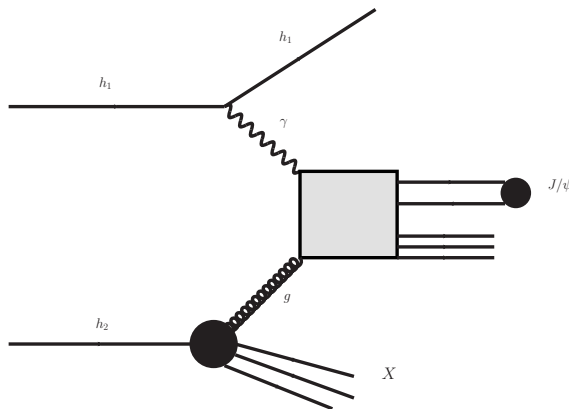


FIG. 1: General diagram for the mechanism of heavy quarkonium production in coherent hadron-hadron interactions at the CERN LHC: $h_1 h_2 \rightarrow h_1 \gamma h_2 \rightarrow h_1 Q(+g) + X$.

number of phenomenological studies on photoproduction have been achieved in [46–50] and references therein. The aim of this paper is to study in detail the inclusive photoproduction of single heavy quarkonium in the NRQCD factorization formalism at the LHC with forward detector acceptances, which is characterized by one rapidity gap in the final state related to the photon exchange, in order to explain the unsuccessfully known inclusive quarkonium mechanism. The study of γ proton and γ Pb as well as $\gamma\gamma$ interactions at the LHC could offer valuable information on the heavy quarkonium production at high energies and more clean backdrop compared to normal hadronic pp, PbPb or Pb p interactions.

The paper is structured into three sections including the introduction in Section I. The detailed description of the hadron tagging devices and the formalism framework for the leading order (LO) cross section of J/ψ production at the LHC are clearly described in Section II. The input parameters and discussed numerical results are shown in Section III. A summary is briefly given in Section IV.

II. SETUP OF THE CALCULATION PROCEDURE

A. Forward hadron tagging

The produced J/ψ meson in pp, PbPb and Pb p collisions is measured in the central detector accompanied by gluon and X. However, the scattered lead and proton remaining intact after collision will not have high transverse momentum and will be difficult to detect with central detector. For that reason, the central detector needs to be

complemented by the installation of the forward hadron detectors which are equipped with charged particle trackers to tag the intact hadrons. The goal of these forward tagging hadron detectors is to catch the undissociated lead and proton after the collision events. They are symmetrically positioned in the region 220 m (420 m) away from the ATLAS and/or CMS interaction points to be 2 mm (5 mm) from the beam [38, 51–53]. These regions cover the range where proton and lead are either both detected at 420 m (symmetric tagging) or one is detected at 220 m and one at 420 m (asymmetric tagging). The forward tagging hadron detectors are characterized by their acceptance, resolution and ability to measure the time-of-flight from interaction point. The resolution and the acceptance of the hadron tagging detector are fixed by the LHC high-luminosity beam optics. The hadron tagging detectors use the FPtract program [54–56] to track the path of the hadrons through the LHC lattice so as to completely find out the acceptance. The acceptance of the forward detectors is controlled by the distance of the active edge of the detector from the beam, which fixes the smallest measurable energy loss of the outgoing hadrons, and the space of the LHC beam elements between the interaction point and the forward detector. The hadrons that lose too much momentum will be absorbed by beam elements, enforcing an upper limit on the measurable momentum loss of hadrons. The hadron tagging technique immediately measures the hadrons surviving the coherent emission.

The suitable forward kinematic variables in hadronic and nuclear reactions are the transverse momentum p_T , the longitudinal momentum p_L , the rapidity y and the polar angle θ . The detector can directly measure the four-momentum of a given final-state produced in the interactions. These momenta and rapidity depend on polar angle with respect to beam axis. The rapidity can be thought of as the relativistically invariant measure of the longitudinal velocity. Pseudorapidity and rapidity are taken equal for negligible masses or highly relativistic particles. Forward rapidity region is the interval where the forward tagging hadron can be detected and is defined beyond $|y| \approx 3$. The produced system can be detected by the central detector at the midrapidity $y \approx 0$. The rapidity gap is large region of pseudorapidity completely devoid of particles, where an intact particle moves at a polar angle θ with respect to the beam [57, 58] and is tagged by forward detector. Moreover, rapidity gaps can also emerge due to fluctuations of the distance between neighbouring particles. A gap in rapidity is present between hadrons and central produced system and one or both interacting hadron stay intact due to the coherent and colorless emission of photon over the hadron. One expects a one-rapidity pattern in the interactions due to the emission of a virtual photon by one of the hadron emerging as undissociated outgoing hadrons at very low angles (few μrad) [59]. The pseudorapidity difference Δy in an event between the intact hadron and the produced system is given as $\Delta y \simeq -\log \xi$. ξ is the fractional longitudinal momentum loss of the outgoing intact hadron [59].

The advantages of forward detectors added to the central detector are to allow the whole reconstruction of the pp, PbPb and Pbp collision events by covering a large range of rapidity, to remove the ambiguity of a rapidity gap tag which suffers from background due to multiplicity events, to veto events (the final state particles in the collision) in which there are no forward rapidity gaps [60–62].

B. Cross Section Formulas

We refer to the heavy quarkonium J/ψ as \mathcal{Q} whereas $h_1 h_2$ is symbolized by pp, PbPb and Pbp or pPb. The cross sections for the $h_1 h_2 \rightarrow h_1 \gamma h_2 \rightarrow h_1 \mathcal{Q}(+g) + X$ process can be expressed as:

$$\sigma(h_1 h_2 \rightarrow h_1 \gamma h_2 \rightarrow h_1 \mathcal{Q}(+g) + X) = \int d\xi dx \sum_n \hat{\sigma}(\gamma g \rightarrow Q\bar{Q}[n](+g) + X) \langle 0 | \mathcal{O}_{1,8}^{J/\psi}[n] | 0 \rangle [f_{\gamma/h_1}(\xi) G_{g/h_2}(x, \mu_f) + h_1 \leftrightarrow h_2], \quad (1)$$

where $\langle 0 | \mathcal{O}_{1,8}^{J/\psi}[n] | 0 \rangle$ is the long-distance matrix element which describes the hadronization of the $Q\bar{Q}$ heavy pair into the physical observable quarkonium state J/ψ . The $\hat{\sigma}(\gamma g \rightarrow Q\bar{Q}[n](+g))$ denotes the short-distance cross section for the partonic process $\gamma g \rightarrow Q\bar{Q}[n](+g)$, which is found by operating the covariant projection method. The Fock state n is given as follows: $^1S_0^{[8]}, ^3P_0^{[8]}, ^3P_2^{[8]}$ for $\gamma g \rightarrow Q\bar{Q}[n]$ partonic $2 \rightarrow 1$ subprocess, and $^3S_1^{[1]}, ^1S_0^{[8]}, ^3S_1^{[8]}, ^3P_0^{[8]}, ^3P_1^{[8]}, ^3P_2^{[8]}$ for $\gamma g \rightarrow Q\bar{Q}[n] + g$ partonic $2 \rightarrow 2$ subprocess. The $G_{g/h_2}(x, \mu_f)$ stands for the gluon parton density function while x , Bjorken variable, is the momentum fraction of the hadron (proton and lead) momentum carried by the gluon. The nuclear gluon distribution is given by $xG_{g/Pb}(x, \mu_f) = A \cdot R_g \cdot xG_{g/p}(x, \mu_f)$, where R_g is the nuclear modification factor for gluon taking into account the nuclear shadowing effects [63] as given by the EPS09 parametrization [64], which is based on a global fit of the current nuclear data. $R_g = 1$ disregards the shadowing corrections. $xG_{g/p}(x, \mu_f)$ is the proton-gluon distribution.

A considerable fraction of pp, PbPb and Pbp collisions at the LHC will include quasi-real (low- Q^2) photon interactions, which is called the photon induced processes. The photon induced interactions have three processes at the LHC with forward detector: (1) photon-photon process, (2) photon-proton process, (3) photon-lead process. In these processes, the emitted photon from the electromagnetic field of one of the two colliding hadrons can interact with

one photon of the other proton or lead (photon-photon process) or directly with the other hadrons (photon-proton process or photon-lead process). This photon from the hadron will have energy E_γ . Consequently, the hadron which emits the photon should have some momentum fraction loss ξ , which is defined as the forward detector acceptance. The ratio between scattered low- Q^2 photons E_γ and incoming energy E is symbolized by $\xi = E_\gamma/E$. The fundamental concept is that the electromagnetic interaction is supposed to dominate at large impact ($b > R_A + R_B$, where R_A and R_B are the hadron radii) and ultrarelativistic energies. In the heavy ion collisions, the heavy nuclei generate strong electromagnetic fields as a result of the coherent action of all protons in the nucleus, which can interact with each other. The analytic estimate for the equivalent photon flux of a hadron, Pb or p, can be evaluated considering the requirement that photoproduction is not followed by hadronic interaction (ultra-peripheral collisions), which is given by [45]

$$f_{\gamma/h}(\xi) = \frac{Z^2 \alpha_{\text{em}}}{\pi \xi} \left[(4a + 1) \ln\left(1 + \frac{1}{a}\right) - \frac{24a^2 + 42a + 17}{6(a + 1)^2} \right], \quad (2)$$

where h can be either p ($Z = 1$) or Pb ($Z = 82$), $a = (\omega/\Lambda_h \gamma)^2$, $\omega = \frac{\sqrt{s}}{2} \xi$ with $\Lambda_p \approx 0.20 \times e^{\frac{17}{12}}$ GeV and $\Lambda_{\text{Pb}} = 80$ MeV [65]. In considering the partonic processes $\gamma(p_1) + g(p_2) \rightarrow Q\bar{Q}[n](p_3) + g(p_4)$, there are eight diagrams for

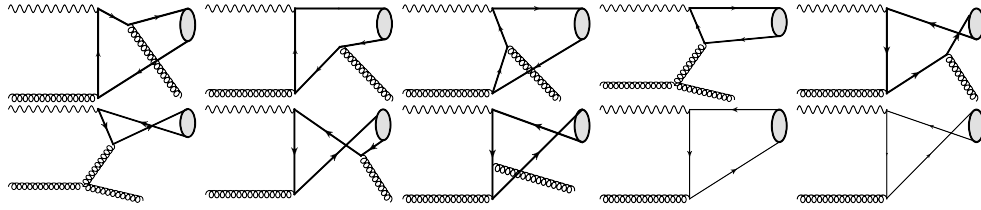


FIG. 2: Feynman diagrams for partonic processes $\gamma + g \rightarrow Q\bar{Q}[n] + g$ (a) and $\gamma + g \rightarrow Q\bar{Q}[n]$ (b).

$\gamma g \rightarrow Q\bar{Q}[n] + g$ and the last two ones are for $\gamma g \rightarrow Q\bar{Q}[n]$. The Feynman diagrams for both processes are shown in Fig. 2.

In pp, PbPb and pPb interactions, the total cross section for $2 \rightarrow 2$ and $2 \rightarrow 1$ subprocesses can be factorized in terms of the equivalent flux of photons into the hadron (p or Pb) projectile and the photon-target production cross section:

a. $h_1 h_2 = \text{pp or PbPb}$. For the $h_1 h_2 \rightarrow h_1 \gamma h_2 \rightarrow h_1 Q(+g) + X$ process where the incident particles are similar, the photon is emitted by one of the incoming particle p(or Pb) and the gluon by the other incoming particle p(or Pb). The final total cross section for $h_1 h_2 \rightarrow h_1 \gamma h_2 \rightarrow h_1 Q + g + X$ process can be now written as:

$$\sigma(h_1 h_2 \rightarrow h_1 \gamma h_2 \rightarrow h_1 Q + g + X) = \int \frac{1}{16\pi^2 x \xi s^2} \frac{p_T^{J/\psi}}{\xi - \frac{m_T^{J/\psi}}{\sqrt{s}} e^{-y^{J/\psi}}} \frac{1}{N_{\text{col}} N_{\text{pol}}} \overline{\sum} |\mathcal{A}_{S,L}|^2 [f_{\gamma/h_1}(\xi) G_{g/h_2}(x, \mu_f) + (h_1 \leftrightarrow h_2)] dp_T^{J/\psi} d\phi^{J/\psi} dy^{J/\psi} d\xi, \quad (3)$$

with x fixed by $x = \frac{1}{\sqrt{s}}(m_T^{J/\psi} e^{y^{J/\psi}} + m_{T\text{e}}^{y_4})$ where $y_4 = -\log(\frac{\sqrt{s}\xi}{m_T^{J/\psi}} - e^{-y^{J/\psi}})$. The final total cross section for $h_1 h_2 \rightarrow h_1 \gamma h_2 \rightarrow h_1 Q + X$ process can also be expressed as:

$$\sigma(h_1 h_2 \rightarrow h_1 \gamma h_2 \rightarrow h_1 Q + X) = \int \frac{\pi p_T^{J/\psi}}{s^2 x \xi^2} \frac{1}{N_{\text{col}} N_{\text{pol}}} \overline{\sum} |\mathcal{A}_{S,L}|^2 [f_{\gamma/h_1}(\xi) G_{g/h_2}(x, \mu_f) + (h_1 \leftrightarrow h_2)] dp_T^{J/\psi} d\phi^{J/\psi} d\xi, \quad (4)$$

with x given by $x = (m_T^{J/\psi})^2 / (s\xi)$.

b. $h_1 h_2 = \text{Pbp or pPb}$. For the $h_1 h_2 \rightarrow h_1 \gamma h_2 \rightarrow Q(+g)h_1 + X$ process where the incident particles are different, the final total cross section is split into two cases: the first case the photon comes from lead and the proton emits gluon (denoted as γp collision); the second case takes place with the exchange of Pbp to pPb, the photon originates from proton and lead emits gluon (denoted as γPb collision). The expression of cross section is arranged in the same way as defined in Eq. 3 (Eq. 4).

In these formulas, ξ is integrated in the region $\xi_{\text{min}} < \xi < \xi_{\text{max}}$ and $\xi_{\text{min}}(\xi_{\text{max}})$ is the lower(upper) limit of forward detector acceptance. The s and m_Q are respectively the square of center-of-mass energy of collider and the mass of heavy quark. The heavy quark represents the charm quark in our study. $p_T^{J/\psi}$, $y^{J/\psi}$, $m_T^{J/\psi}$, $\phi^{J/\psi}$ are the transverse momenta, rapidity, transverse mass and azimuthal angle of the charmonium where $m_T^{J/\psi} = \sqrt{(p_T^{J/\psi})^2 + (m_{J/\psi})^2}$.

m_{4T} and y_4 are the transverse mass and rapidity of gluon, respectively. Similarly as in photoproduction induced by electron proton collisions, we can define the $z^{J/\psi}$ parameter $z^{J/\psi} = P_h \cdot P^{J/\psi} / P_h \cdot q_\gamma$ where P_h , q_γ , $P^{J/\psi}$ are the momenta of the hadron, the virtual photon and charmonium, respectively. The data are somehow taken in either inelastic or elastic regime. The inelastic regime is commonly considered to be the area where z is below 0.8 or 0.9 while the elastic regime is considered to be the area near $z^{J/\psi} = 1$ [33]. The gluon shadowing is interpreted in the nuclear infinite momentum frame as a result of fusion of gluons originating from different bound nucleons [66]. The fundamental form of gluon shadowing is gluon saturation [67]. The nuclear shadowing effect manifests itself in PbPb and γ Pb interactions where the nucleus emits the gluon while pp and γ p interactions don't reveal this effect.

The summations in Eqs.(3) and (4) are taken over the spins and colors of initial and final states, and the bar over the summation denotes averaging over the spins and colors of initial parton. The Mandelstam variables are defined as $\hat{s} = (p_1 + p_2)^2$, $\hat{t} = (p_1 - p_3)^2$ and $\hat{u} = (p_1 - p_4)^2$. N_{col} and N_{pol} refer to as the numbers of colors and polarization of states n , separately. The QCD amplitudes with amputated heavy-quark spinors read as follows [68]:

$$\begin{aligned} \mathcal{A}_{Q\bar{Q}}[{}^1S_0^{(1/8)}] &= \text{Tr}[\mathcal{C}_{(1/8)}\Pi_0\mathcal{A}]_{q=0}, \\ \mathcal{A}_{Q\bar{Q}}[{}^3S_1^{(1/8)}] &= \epsilon_\alpha \text{Tr}[\mathcal{C}_{(1/8)}\Pi_1^\alpha\mathcal{A}]_{q=0}, \\ \mathcal{A}_{Q\bar{Q}}[{}^1P_1^{(1/8)}] &= \epsilon_\beta \frac{d}{dq_\beta} \text{Tr}[\mathcal{C}_{(1/8)}\Pi_0\mathcal{A}]_{q=0}, \\ \mathcal{A}_{Q\bar{Q}}[{}^1P_J^{(1/8)}] &= \epsilon_{\alpha\beta}^{(J)} \frac{d}{dq_\beta} \text{Tr}[\mathcal{C}_{(1/8)}\Pi_1^\alpha\mathcal{A}]_{q=0}, \end{aligned} \quad (5)$$

where \mathcal{A} denotes the QCD amplitude with amputated heavy-quark spinors, the lower index q represents the momentum of the heavy-quark in the $Q\bar{Q}$ rest frame. $\Pi_{0/1}$ are spin projectors onto spin singlet and spin triplet states stated as

$$\begin{aligned} \Pi_0 &= \frac{1}{\sqrt{8m_Q^3}} \left(\frac{\not{P}}{2} - \not{q} - m_Q \right) \gamma_5 \left(\frac{\not{P}}{2} + \not{q} + m_Q \right), \\ \Pi_1^\alpha &= \frac{1}{\sqrt{8m_Q^3}} \left(\frac{\not{P}}{2} - \not{q} - m_Q \right) \gamma^\alpha \left(\frac{\not{P}}{2} + \not{q} + m_Q \right), \end{aligned} \quad (6)$$

where P is the total momentum of heavy quarkonium and q is the relative momentum between the $Q\bar{Q}$ pair. $\mathcal{C}_{1/8}$ are color factor projectors onto the color-singlet and color-octet states and can be expressed as follows:

$$\begin{aligned} C_1 &= \frac{\delta_{ij}}{\sqrt{N_c}}, \\ C_8 &= \sqrt{2} T_{ij}^c, \end{aligned} \quad (7)$$

where N_c is the number of color, and T_{ij}^c is the generator of $SU(N_c)$, and i, j are color indices for the heavy quarks. The summation over the polarization is given as:

$$\begin{aligned} \sum_{J_z} \varepsilon_\alpha \varepsilon_{\alpha'}^* &= \Pi_{\alpha\alpha'}, \\ \sum_{J_z} \varepsilon_{\alpha\beta}^0 \varepsilon_{\alpha'\beta'}^{0*} &= \frac{1}{3} \Pi_{\alpha\beta} \Pi_{\alpha'\beta'}, \\ \sum_{J_z} \varepsilon_{\alpha\beta}^1 \varepsilon_{\alpha'\beta'}^{1*} &= \frac{1}{2} (\Pi_{\alpha\alpha'} \Pi_{\beta\beta'} - \Pi_{\alpha\beta'} \Pi_{\alpha'\beta}), \\ \sum_{J_z} \varepsilon_{\alpha\beta}^2 \varepsilon_{\alpha'\beta'}^{2*} &= \frac{1}{2} (\Pi_{\alpha\alpha'} \Pi_{\beta\beta'} + \Pi_{\alpha\beta'} \Pi_{\alpha'\beta}) - \frac{1}{3} \Pi_{\alpha\beta} \Pi_{\alpha'\beta'}, \end{aligned} \quad (8)$$

where ε_α ($\varepsilon_{\alpha\beta}$) represents the polarization vector (tensor) of the $Q\bar{Q}$ states, and $\Pi_{\alpha\beta} = -g_{\alpha\beta} + \frac{P_\alpha P_\beta}{M_{J/\psi}^2}$, and $M_{J/\psi}$ is the J/ψ mass. The amplitude squares multiplied by long distance matrix elements are listed in the appendix A.

III. NUMERICAL RESULTS AND DISCUSSION

In this section, we discuss the numerical results of the photoproduction of J/ψ by using some physical parameters. $M_p = 0.94$ GeV is the mass of proton. The mass of the heavy quark is chosen as $m_Q = 1.5$ GeV where Q represents the

charm quark in our case. The mass of J/ψ is literally put at $M_{J/\psi} = 2m_Q$. The colliding energies used in this paper are $\sqrt{s}=14$ TeV for pp, and $\sqrt{s}=5$ TeV for PbPb and Pbp. CTEQ6L1 [69] is used for the proton-gluon distribution which is probed at the factorization scale chosen as $\mu_f = m_T^{J/\psi}$, where $m_T^{J/\psi} = \sqrt{(p_T^{J/\psi})^2 + M_{J/\psi}^2}$ is the transverse mass. The minimum value of the transverse momentum of the quarkonium is chosen at $p_{T\min}^Q = 1$ GeV. The range of $z^{J/\psi}$ is selected from zero to the area near one ($z^{J/\psi} < 1$) and the predictions are not strongly dependent on the inferior limit of the integration $z_{\min}^{J/\psi}$ [70]. Numerical calculations are carried out by in-house monte carlo generator. The choice of the LDMEs for J/ψ is taken from [71] as shown in Table I. For $\langle 0 | \mathcal{O}_8^{J/\psi}({}^3P_J) | 0 \rangle$ with $J=0,1,2$, and

$\langle 0 \mathcal{O}_{1,8}^{J/\psi}({}^{2S+1}L_J) 0 \rangle$	Numerical value
$\langle 0 \mathcal{O}_1^{J/\psi}({}^3S_1) 0 \rangle$	1.16 GeV^3
$\langle 0 \mathcal{O}_8^{J/\psi}({}^3S_1) 0 \rangle$	$0.3 \times 10^{-2} \text{ GeV}^3$
$\langle 0 \mathcal{O}_8^{J/\psi}({}^1S_0) 0 \rangle$	$8.9 \times 10^{-2} \text{ GeV}^3$
$\langle 0 \mathcal{O}_8^{J/\psi}({}^3P_0) 0 \rangle$	$1.26 \times 10^{-2} \text{ GeV}^5$

TABLE I: Numerical values of LDMEs.

following the heavy-quark spin symmetry, we get the relations:

$$\langle 0 | \mathcal{O}_8^{J/\psi}({}^3P_J) | 0 \rangle = (2J+1) \langle 0 | \mathcal{O}_8^{J/\psi}({}^3P_0) | 0 \rangle. \quad (9)$$

$\sigma[\text{nb}] \setminus \xi_i$	$0.015 < \xi_3 < 0.15$		$0.0015 < \xi_2 < 0.5$		$0.1 < \xi_1 < 0.5$		$0 < \xi < 1$	
	with-s	no-s	with-s	no-s	with-s	no-s	with-s	no-s
$\sigma_{2 \rightarrow 1}^{\text{pp}}$	-	4.71×10^1	-	1.20×10^2	-	1.17×10^1	-	2.45×10^2
$\sigma_{2 \rightarrow 1}^{\text{pbpb}}$	1.92×10^6	2.75×10^6	1.73×10^7	2.41×10^7	2.58×10^3	3.79×10^3	6.41×10^7	7.93×10^7
$\sigma_{2 \rightarrow 1}^{\gamma \text{Pb}}$	4.45×10^3	6.43×10^3	1.13×10^4	1.60×10^4	1.09×10^3	1.61×10^3	2.20×10^4	2.88×10^4
$\sigma_{2 \rightarrow 1}^{\gamma \text{p}}$	-	1.32×10^4	-	1.16×10^5	-	1.82×10^1	-	3.81×10^5
$\sigma_{2 \rightarrow 2}^{\text{pp}}$	-	4.56×10^1	-	1.07×10^2	-	1.23×10^1	-	1.66×10^2
$\sigma_{2 \rightarrow 2}^{\text{pbpb}}$	1.56×10^6	1.98×10^6	1.20×10^7	1.46×10^7	2.39×10^3	3.15×10^3	2.78×10^7	3.12×10^7
$\sigma_{2 \rightarrow 2}^{\gamma \text{Pb}}$	3.78×10^3	4.88×10^3	8.68×10^3	1.09×10^4	1.03×10^3	1.38×10^3	1.25×10^4	1.50×10^4
$\sigma_{2 \rightarrow 2}^{\gamma \text{p}}$	-	9.52×10^3	-	7.01×10^4	-	1.52×10^1	-	1.50×10^5

TABLE II: The total cross section (nb) for the J/ψ photoproduction with nuclear shadowing effect (with – s) and without nuclear shadowing effect (no – s) effect at LHC with forward detector acceptances.

In Table II, we present our estimates for the total cross sections of J/ψ photoproduction including both $2 \rightarrow 1$ and $2 \rightarrow 2$ subprocesses at LHC with forward detector acceptances. We consider the pp, PbPb and Pbp collisions where Pbp means gluon can be emitted from proton (γp) or lead (γPb). The nuclear shadowing effect is included only when gluons are emitted from nucleus. Our predictions show that the total cross sections with ξ_2 and ξ_3 are close and keep more contribution to J/ψ photoproduction than ξ_1 . The $2 \rightarrow 1$ subprocess produces only color octet channels. The $2 \rightarrow 2$ subprocess generates color octet channels as well as the color singlet channel due to the emission of gluon. The color singlet and color octet ${}^1S_0^{[8]}$ channels have dominantly contributed to the total cross section. These two contributions have enhanced the total cross section of the $2 \rightarrow 2$ subprocess. However, its total cross sections are small in most cases with reference to $2 \rightarrow 1$ because of the two-body final state phase space suppression. Notice here we have applied a $p_{T\min}^Q = 1$ GeV cut for $2 \rightarrow 2$ production. It has been found that the total cross sections with nuclear shadowing effect are lower than those without nuclear shadowing effect. The reduction is due to nuclear modification of the parton distribution functions [72, 73] and the decrease of the gluon density in the nucleus at low depletion of Bjorken variable at $x \lesssim 0.1$ [66]. In certain case, the production of charmonium can be altered by nuclear matter effect such as parton energy loss due to multiple scattering in the nucleus [74]. It has also been shown that the cross section of PbPb interactions is larger than that of Pbp and pp interactions, Pbp interactions is larger than that of pp, which can be accounted for by the enhancement of the photon flux from nuclei and the gluon distribution from lead, i.e., proportional to Z^2 and A .

In Table III, we predict the dominant total cross sections of pp, PbPb and Pbp collisions and the cross sections of different color octet and color singlet contributions including both $2 \rightarrow 1$ and $2 \rightarrow 2$ with and without shadowing effect for the J/ψ photoproduction at the LHC with forward detector acceptances $0.0015 < \xi_2 < 0.5$. We see that the cross section of color-octet channel subprocess contribution ${}^3S_1^{[8]}$ (${}^1S_0^{[8]}$) has a lower (larger) contribution to the total ones.

$\sigma[\text{nb}]$	$0.0015 < \xi_2 < 0.5$			
	pp	PbPb	γp	γPb
$2 \rightarrow 1$ total	1.20×10^2	1.73×10^7	1.16×10^5	1.13×10^4
$2 \rightarrow 2$ total	1.07×10^2	1.20×10^7	7.01×10^4	8.68×10^3
$^3S_1^{[1]}$	4.15×10^0	5.30×10^5	3.36×10^3	3.57×10^2
$^1S_0^{[8]}$	7.66×10^1	8.57×10^6	4.99×10^4	6.23×10^3
$^3S_1^{[8]}$	0.02×10^0	2.57×10^3	1.63×10^1	1.73×10^0
$^3P_0^{[8]}$	9.25×10^0	1.04×10^6	6.10×10^3	7.55×10^2
$^3P_1^{[8]}$	3.69×10^0	4.01×10^5	2.30×10^3	2.97×10^2
$^3P_2^{[8]}$	1.29×10^1	1.44×10^6	8.36×10^3	1.05×10^3

TABLE III: The total cross sections of pp, PbPb and Pbp collisions where Pbp means gluon can be emitted from proton (γp) or lead (γPb), and the cross sections of different color octet and color singlet subprocesses contributions with and without nuclear shadowing effect for the J/ψ photoproduction at the LHC with forward detector acceptances ξ_2 .

$N \setminus \xi_i$	$\mathcal{L}_{\text{LHC}}[\text{mb}^{-1}\text{s}^{-1}]$	$T[\text{s}]$	$0.0015 < \xi_2 < 0.5$	
			with-s	no-s
$N_{2 \rightarrow 1}^{\text{pp}}$	10^7	10^7	-	1.2×10^{10}
$N_{2 \rightarrow 1}^{\text{pbpb}}$	0.42	10^6	7.23×10^6	1.01×10^7
$N_{2 \rightarrow 1}^{\gamma\text{Pb}}$	150	10^6	1.70×10^6	2.40×10^6
$N_{2 \rightarrow 1}^{\gamma\text{p}}$	150	10^6	-	1.74×10^7
$N_{2 \rightarrow 2}^{\text{pp}}$	10^7	10^7	-	1.07×10^{10}
$N_{2 \rightarrow 2}^{\text{pbpb}}$	0.42	10^6	5.04×10^6	6.13×10^6
$N_{2 \rightarrow 2}^{\gamma\text{Pb}}$	150	10^6	1.30×10^6	1.64×10^6
$N_{2 \rightarrow 2}^{\gamma\text{p}}$	150	10^6	-	1.05×10^7

TABLE IV: The production rates of pp, PbPb and Pbp interactions of J/ψ photoproduction with nuclear shadowing effect (with-s) and without nuclear shadowing effect (no-s) effect at the LHC with forward detector acceptances $0.0015 < \xi_2 < 0.5$.

In Table IV, we present our estimates for production rates of pp, PbPb and Pbp interactions by assuming the design integrated luminosities $\mathcal{L}_{\text{LHC}}^{\text{pp}}$, $\mathcal{L}_{\text{LHC}}^{\text{PbPb}}$, $\mathcal{L}_{\text{LHC}}^{\text{Pbp}}$ and run times (T) [75]. Our predictions show that the event rates of pp interactions dominate over the event rates of PbPb and Pbp interactions, due to its considerable design integrated luminosity and running time. The design integrated luminosity of Pbp interactions, which are two order of magnitude larger than for PbPb, lessens the suppression for the event rates. Nonetheless, the resulting production rates are still minute in comparison to the pp results. Although the values of the cross sections are considerable, the clean topology of coherent interactions involves a higher signal to background ratio. Hence, the experimental detection is evidently possible. The main drawback is that the signal is supposed to be downgraded due to the event pileup. An option to rate coherent events at the LHC is by tagging the intact hadron in the final state.

$N \setminus \xi_i$	$\mathcal{L}_{\text{LHC}}[\text{mb}^{-1}\text{s}^{-1}]$	$T[\text{s}]$	$0.0015 < \xi_2 < 0.5$	
			with-s	no-s
$N_{2 \rightarrow 1}^{\gamma\text{Pb}}$	10^4	10^7	1.13×10^9	1.60×10^9
$N_{2 \rightarrow 1}^{\gamma\text{p}}$	10^4	10^7	-	1.16×10^{10}
$N_{2 \rightarrow 2}^{\gamma\text{Pb}}$	10^4	10^7	8.68×10^8	1.09×10^9
$N_{2 \rightarrow 2}^{\gamma\text{p}}$	10^4	10^7	-	7.01×10^9

TABLE V: The production rate of Pbp interactions of J/ψ photoproduction with nuclear shadowing effect (with-s) and without nuclear shadowing effect (no-s) effect at upgraded LHC with forward detector acceptances $0.0015 < \xi_2 < 0.5$.

As for Pbp interactions, an enhanced setup was suggested in Ref.[76] and the design integrated luminosity $\mathcal{L}_{\text{LHC}}^{\text{Pbp}}$ and the running time (T) were upgraded. The upgraded production rates are arranged in Table V and our estimate reveals that the main upgraded production rates hail from γp interactions because of the large cross sections. Therefore, the experimental analysis can be made possible with the upgraded event rates of γp interactions due to the fact that the numbers are reasonable and those collisions are supposed to trigger on and perform the measurement with almost no pileup. For that reason, the upgraded γp scenarios give one of the best feasibilities to detect the inelastic J/ψ

photoproduction in coherent processes.

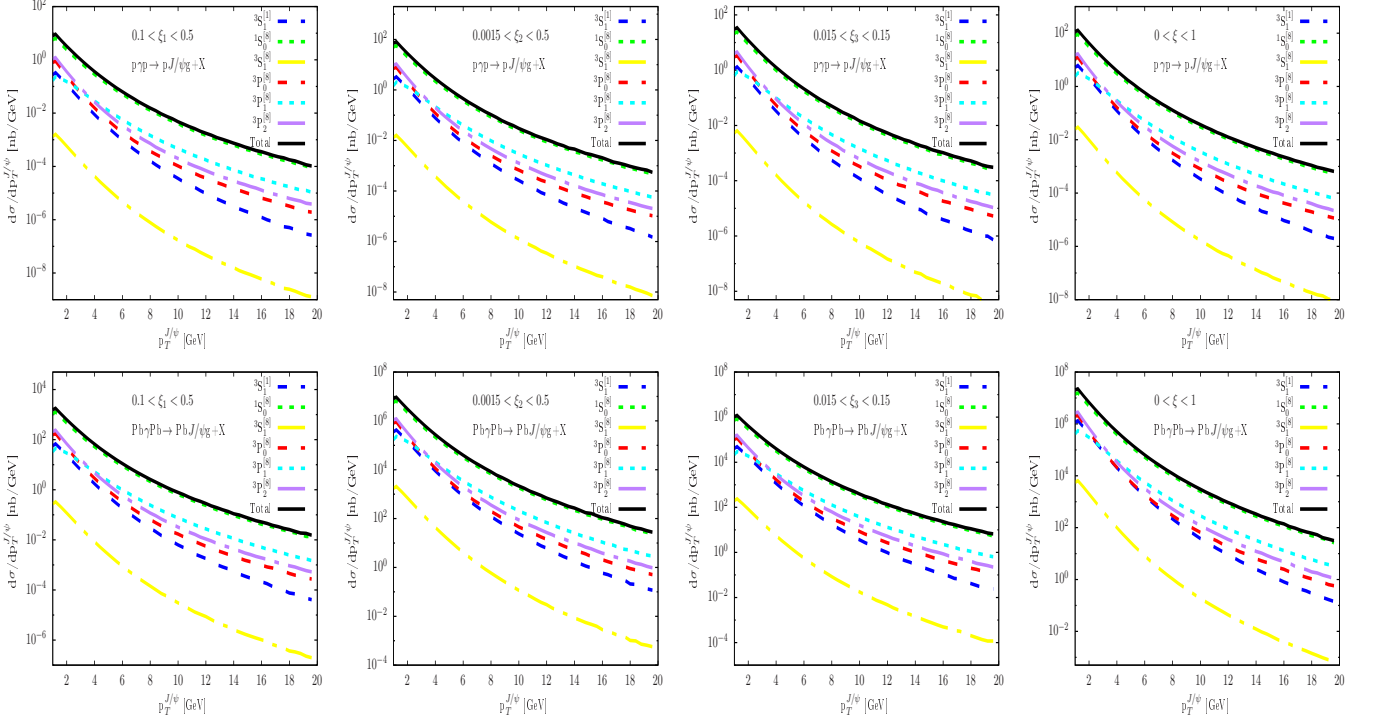


FIG. 3: (color online) The $p_T^{J/\psi}$ distributions for the $p\gamma p \rightarrow pQg + X$ (top panel) and $Pb\gamma Pb \rightarrow PbQg + X$ (bottom panel) processes, and the contributions of the $^3S_1^{[1]}$ (blue dashed line), $^1S_0^{[8]}$ (green dotted line), $^3S_1^{[8]}$ (yellow dash dotted line), $^3P_0^{[8]}$ (red dashed line), $^3P_1^{[8]}$ (cyan dotted line), $^3P_2^{[8]}$ (purple dash dotted line) channels and Total (black solid line).

The values of scaling variable $p_T^{J/\psi}$ can be used to choose the appropriate models of quarkonia production. At small transverse momentum, the CSM is usually used to explain the J/ψ photoproduction. However, the CO mechanism and the fragmentation approach are preferentially selected at large transverse momentum to address the quarkonia production. In Figs.3 and 4, we plot the predictions of the $p_T^{J/\psi}$ distributions in pp, PbPb and Pbp collisions with $0.1 < \xi_1 < 0.5$ for CMS-TOTEM forward detector, $0.0015 < \xi_2 < 0.5$ for CMS-TOTEM forward detector, $0.015 < \xi_3 < 0.15$ for AFP-ATLAS forward detector and $0 < \xi < 1$ for different Fock state contributions. The pPb collision is split into $p\gamma Pb \rightarrow pJ/\psi(+g) + X$ which signifies the initial photon is emitted from proton while this proton stays undissociated in the final state (γPb interaction) and $p\gamma Pb \rightarrow J/\psi Pb(+g) + X$ which signifies the initial photon is emitted from lead while this lead stays undissociated (γp interaction). The forward $p_T^{J/\psi}$ contribution is only considered in this case study, meanwhile γPb and γp interactions are separately described. The total contribution will be two times larger if backward is included in PbPb and pp interactions, and sum of the two in Pbp interaction. The $p_T^{J/\psi}$ distributions show that the color-octet and color-singlet channels have a similar peak in small- $p_T^{J/\psi}$ region at $p_T^{J/\psi} \approx m_Q$. From that point, they start decreasing and dropping down logarithmically. Indeed, at moderate transverse momentum $p_T^{J/\psi} \geq m_Q$, the J/ψ photoproduction has much milder slope. The color-octet channels $^3S_1^{[8]}$, $^3P_0^{[8]}$, $^3P_2^{[8]}$ and the color-singlet channel $^3S_1^{[1]}$ drop much faster than the color-octet channels $^1S_0^{[8]}$ and $^3P_1^{[8]}$ with the increase of $p_T^{J/\psi}$. The slopes of $^3P_1^{[8]}$ and $^1S_0^{[8]}$ are small different from others. From our description, it has been observed that the $p_T^{J/\psi}$ distribution decreases with $p_T^{J/\psi}$ following a power law behavior proportional to $1/(P_T^{J/\psi})^n$ where n being energy dependent and different for each meson stands for the effective power. The color-octet channel $^1S_0^{[8]}$ dominates over the other color-octet and color-singlet contributions in small and large $p_T^{J/\psi}$ regions which provides the main contribution to the $p_T^{J/\psi}$ distribution of photoproduction processes, while the color-octet channel $^3S_1^{[8]}$ gives the low one. Certain processes for example diffraction [77] and fragmentation [78, 79] can also contribute to $p_T^{J/\psi}$ distribution at small $p_T^{J/\psi}$ and with very small total cross section, respectively. These two processes have not been taken into account and will be studied in our future work.

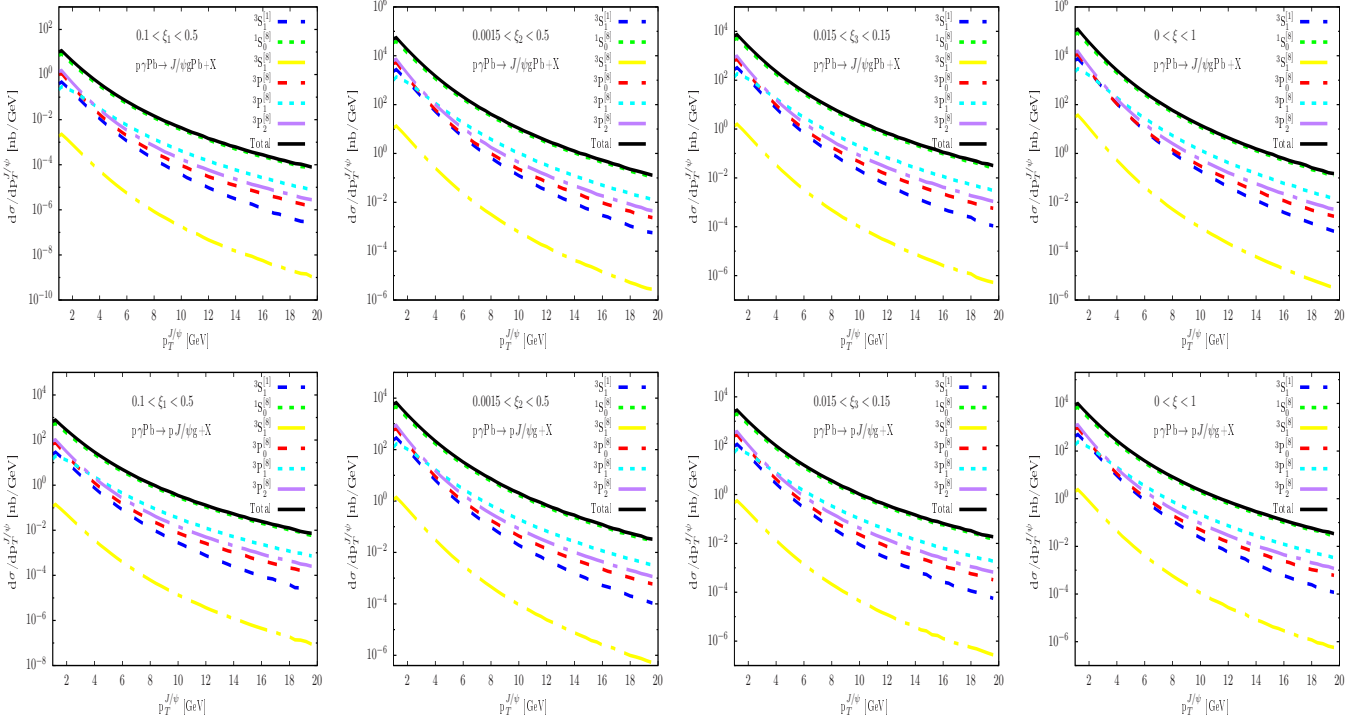


FIG. 4: (color online) The $p_T^{J/\psi}$ distributions for the $p\gamma\text{Pb} \rightarrow Qg\text{Pb} + X$ (top panel) and $p\gamma\text{Pb} \rightarrow pQg + X$ (bottom panel) processes, and the contributions of the $^3S_1^{[1]}$ (blue dashed line), $^1S_0^{[8]}$ (green dotted line), $^3S_1^{[8]}$ (yellow dash dotted line), $^3P_0^{[8]}$ (red dashed line), $^3P_1^{[8]}$ (cyan dotted line), $^3P_2^{[8]}$ (purple dash dotted line) channels and Total (black solid line).

The values of scaling variable $z^{J/\psi}$ can be used for the separation of the elastic, inelastic and diffractive photoproduction events in $z^{J/\psi}$ distributions. The $2 \rightarrow 1$ subprocess cross section vanishes except $z^{J/\psi} = 1$ and contributes to J/ψ photoproduction in forward direction which means that the pp, PbPb, Pbp collisions in $2 \rightarrow 1$ subprocess don't have the total contribution in the region $0 < z^{J/\psi} < 0.9$ and nearly vertically increase at the endpoint $z^{J/\psi} = 1$. However, the total contributions for $2 \rightarrow 2$ subprocess increase along with $z^{J/\psi}$ in the region $0 < z^{J/\psi} < 0.9$ and drastically increase obliquely for $0.9 < z^{J/\psi} < 1$. Here, the forward distribution is only regarded and the Pbp collision is divided into two. The total $z^{J/\psi}$ distribution will be twofold larger in pp and PbPb collisions and the sum of the two in Pbp collisions if the backward distribution is involved. In Figs. 5 and 6, we present our prediction for $z^{J/\psi}$ distributions and it has been observed that the color-singlet channel $^3S_1^{[1]}$ and the color octet channel $^3S_1^{[8]}$ begin to increase lightly and go down logarithmically with the increase of $z^{J/\psi}$. The other remaining color octet channels also begin to increase lightly and drastically going up logarithmically along with $z^{J/\psi}$. The color-singlet channel gives the main contribution in the region of $0 < z^{J/\psi} < 0.5$ while the color octet channel $^1S_0^{[8]}$ provides the main one in the region of $z^{J/\psi} > 0.5$. The low contribution to the $z^{J/\psi}$ distribution comes from the color octet channel $^3S_1^{[8]}$ as $z^{J/\psi}$ enlarges. In our work, we have only considered the direct photon process produced from proton or lead in the inelastic process, and our J/ψ photoproduction is direct which means that the quarkonium is directly produced in the hard scattering. The feeddown is one of the contributors to the J/ψ spectrum which is expected to originate from higher charmonium states as well as B meson decays [82]. Some processes for instance the single and double resolved J/ψ photoproduction channel can also contribute significantly at small $z^{J/\psi}$ [83–85], and color singlet model is dominant over the photon-gluon fusion [34] as in the direct photon process, whereas the elastic/diffractive process gives contribution to the J/ψ photoproduction at large $z^{J/\psi}$ [77]. The contributions of resolved photoproduction and the diffractive production are in general excluded from experimental measurements due to the unavailability of the data, in order to make a significant comparison [86]. The feed-down contribution (15%) from an excited state $\psi(2S)$ [87] and decay contribution (1%) from χ_{cJ} states [77, 88] to J/ψ photoproduction are not included in our current work. The light quark contribution is expected to be negligible compared to the photon-gluon fusion process [34]. The J/ψ photoproduction cross section to NLO confirmed that the corrections are considerable, enlarging towards large transverse momentum of J/ψ meson [86, 88–90]. For example, the NRQCD cross section of the J/ψ photoproduction

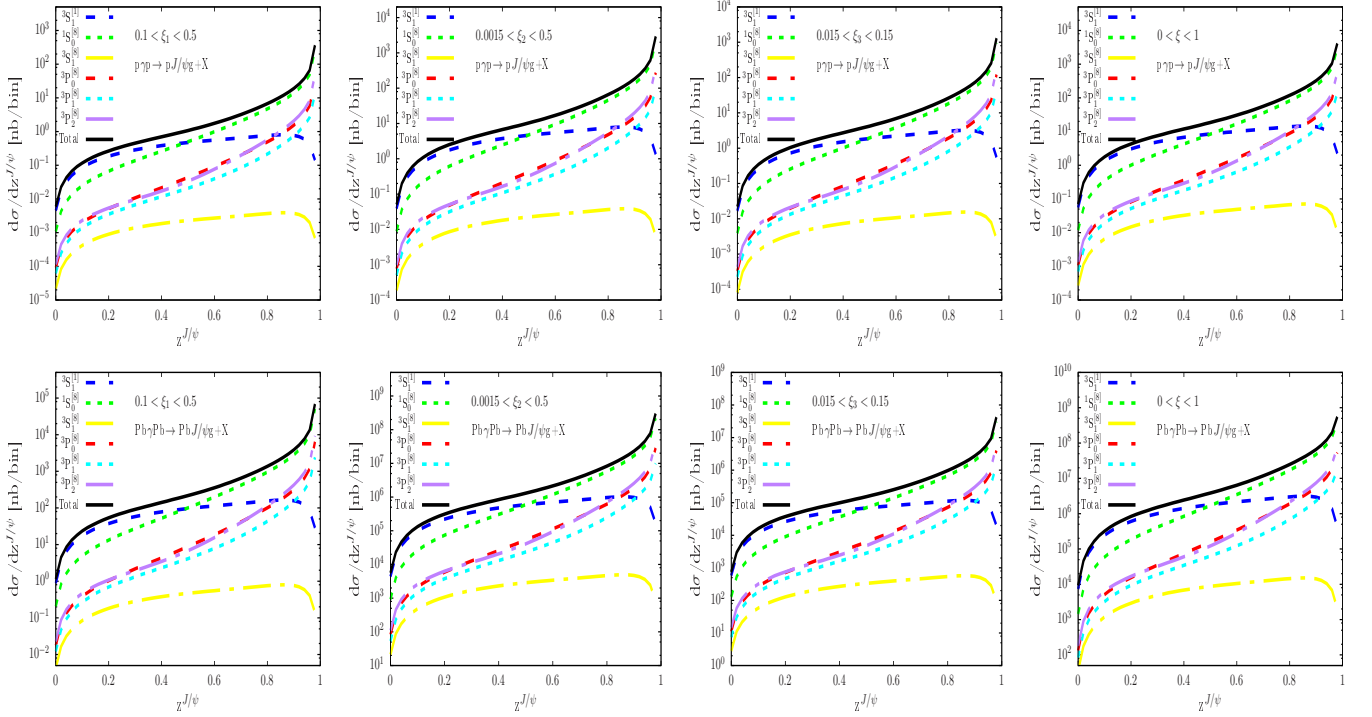


FIG. 5: (color online) The $z^{J/\psi}$ distributions for the $p\gamma p \rightarrow pQg + X$ (top panel) and $Pb\gamma Pb \rightarrow PbQg + X$ (bottom panel) processes, and the contributions of the $^3S_1^{[1]}$ (blue dashed line), $^1S_0^{[8]}$ (green dotted line), $^3S_1^{[8]}$ (yellow dash dotted line), $^3P_0^{[8]}$ (red dashed line), $^3P_1^{[8]}$ (cyan dotted line), $^3P_2^{[8]}$ (purple dash dotted line) channels and Total (black solid line).

to LO can be improved by next to leading order (NLO) corrections up to 115% in the considered kinematic in electron proton collisions through γg fusion[77]. We have commented that NLO has been vital and will need to be considered in future works.

In Fig.7, we exhibit our predictions of the $y^{J/\psi}$ and $\log \xi$ distributions for the inelastic J/ψ photoproduction in coherent pp and PbPb collisions at LHC energies for four different forward detector acceptances. The two first figures on top (bottom) left panel and two last figures on top (bottom) right panel represent the $y^{J/\psi}$ and $\log \xi$ distributions for pp (PbPb) collision in $2 \rightarrow 1$ and $2 \rightarrow 2$ subprocesses. Given the photon flux and colliding energy, the study of the J/ψ photoproduction distributions can be employed to constrain the photoproduction cross section. In the case of pp and PbPb collisions, both incident protons and leads are sources of photons providing equally at forward and backward rapidities, respectively. The forward rapidity is defined by the negative $\phi^{J/\psi}$ and the backward one by the positive $\phi^{J/\psi}$. As a result, the total $y^{J/\psi}$ and $\log \xi$ distributions at forward and backward are symmetric about midrapidity. The forward contribution is only taken into the consideration while total contributions would be two times larger. In the figures on the top (bottom) panels, the $y^{J/\psi}$ and $\log \xi$ distributions for pp (PbPb) collision are computed considering the parametrization for the gluon distribution in the proton (lead). we observe that the shapes of $y^{J/\psi}$ and $\log \xi$ distributions of $2 \rightarrow 1$ subprocess are similar and symmetric. Contrariwise, the shapes of $y^{J/\psi}$ and $\log \xi$ distributions of $2 \rightarrow 2$ subprocess are dissimilar and asymmetric due to the emission of gluon in the final state. The pp and PbPb contributions peak for the negative rapidities as shown in our figures due to the flux of photon in forward rapidities.

Fig.8 shows the $y^{J/\psi}$ and $\log \xi$ distributions for pPb collision where $p\gamma Pb \rightarrow pJ/\psi(+g) + X$ means initial photon is emitted from proton while this proton remains undissociated in the final state (γPb interaction), and $p\gamma Pb \rightarrow J/\psi Pb(+g) + X$ means the initial photon is emitted from lead while this lead remains undissociated (γp interaction). The full contribution to pPb interaction would be the sum of these two while here we split them and study them separately. The two first figures on top (bottom) left panel and two last figures on top (bottom) right panel represent the $y^{J/\psi}$ and $\log \xi$ distributions for Pbp collision in $2 \rightarrow 1$ ($2 \rightarrow 2$) subprocesses. As for Pbp collisions, the $y^{J/\psi}$ and $\log \xi$ distribution at forward and backward are asymmetric about midrapidity due to the differences of the fluxes and parton distribution function. For example, in γp interaction, the photon comes from the nuclei, with photon flux being proportional to Z^2 and the photoproduction cross section is defined by the gluon density of the proton

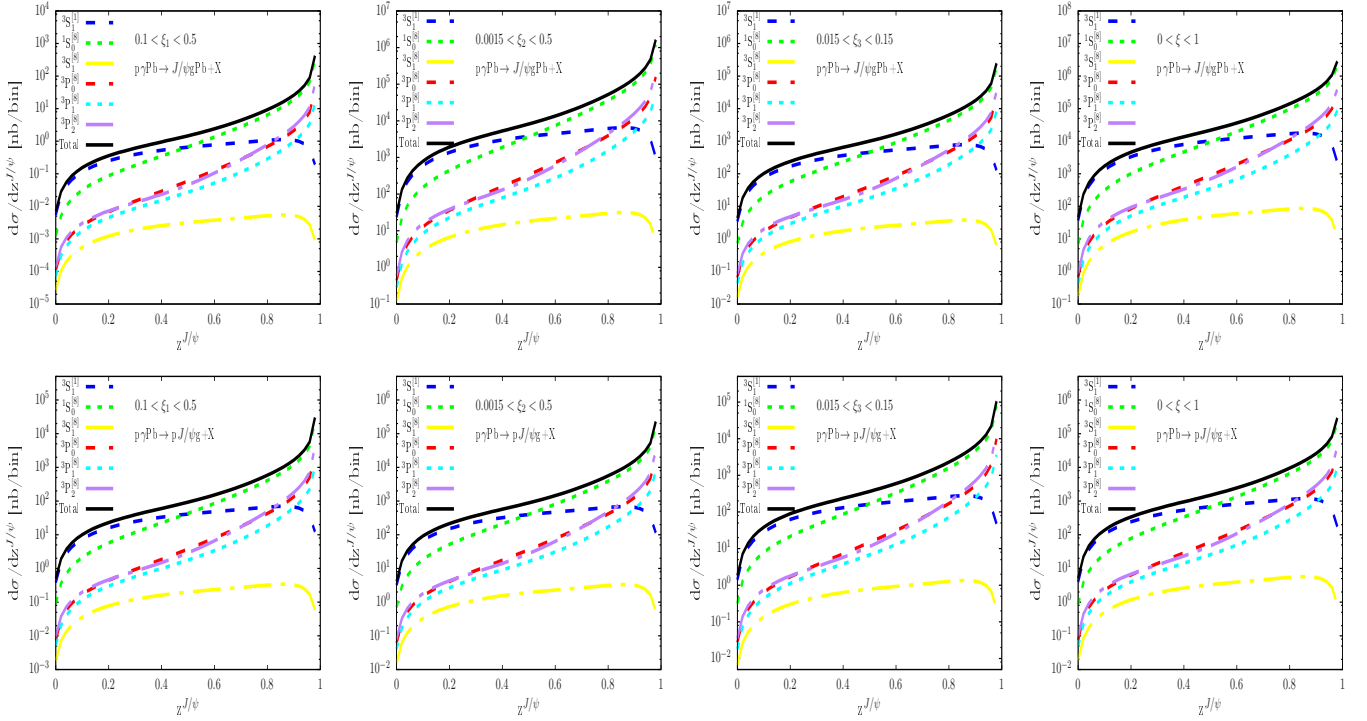


FIG. 6: (color online) The $z^{J/\psi}$ distributions for the $p\gamma Pb \rightarrow Qg Pb + X$ (top panel) and $p\gamma Pb \rightarrow p Qg + X$ (bottom panel) processes, and the contributions of the $^3S_1^{[1]}$ (blue dashed line), $^1S_0^{[8]}$ (green dotted line), $^3S_1^{[8]}$ (yellow dash dotted line), $^3P_0^{[8]}$ (red dashed line), $^3P_1^{[8]}$ (cyan dotted line), $^3P_2^{[8]}$ (purple dash dotted line) channels and Total (black solid line).

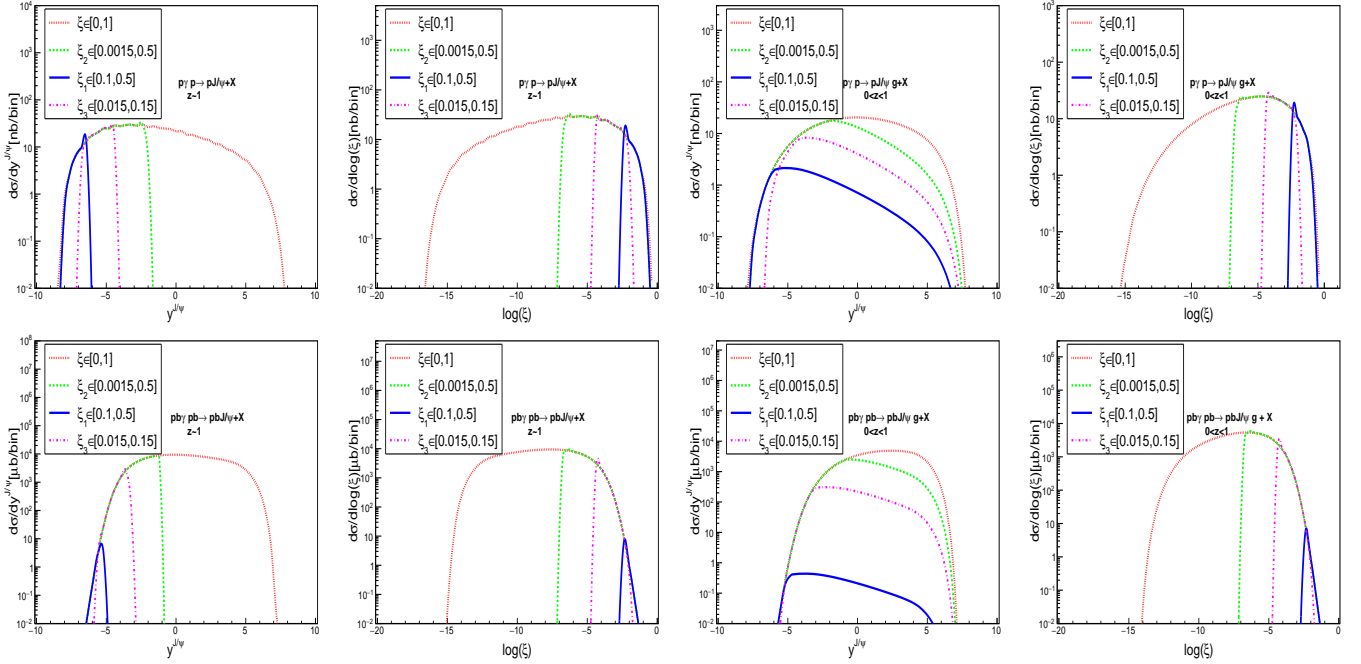


FIG. 7: (color online) The $y^{J/\psi}$ and $\log \xi$ distributions for the $p\gamma p \rightarrow p J/\psi + X$ and $p\gamma p \rightarrow p J/\psi g + X$ processes (top panels) and $Pb\gamma Pb \rightarrow Pb J/\psi + X$ and $Pb\gamma Pb \rightarrow Pb J/\psi g + X$ processes (bottom panels) for the forward detector with ξ (red dashed line), at the CMS-TOTEM forward detector with ξ_1 (green dashed line), at the CMS-TOTEM forward detector with ξ_2 (blue solid line), and at the AFP-ATLAS forward detector with ξ_3 (magenta dash dotted line).

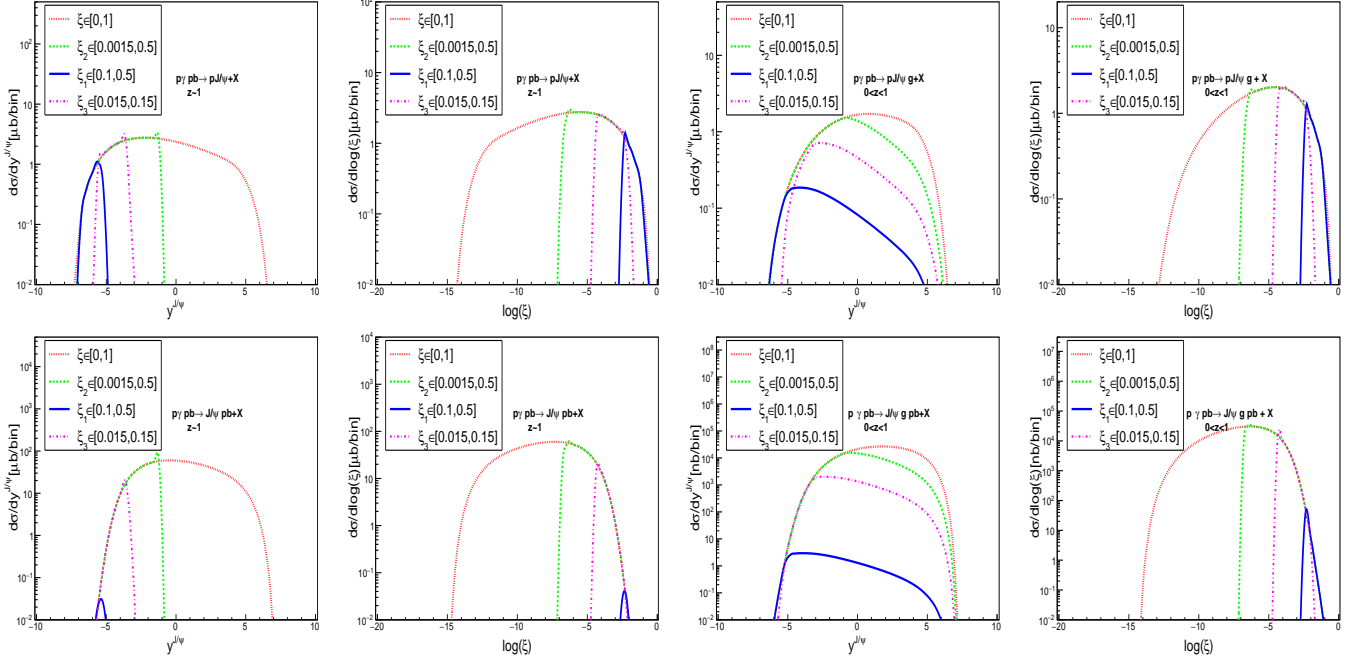


FIG. 8: (color online) The $y^{J/\psi}$ and $\log \xi$ distributions with nuclear shadowing effect for the $p\gamma\text{Pb} \rightarrow pJ/\psi + X$ and $p\gamma\text{Pb} \rightarrow pJ/\psi g + X$ processes (top panels) and $p\gamma\text{Pb} \rightarrow J/\psi\text{Pb} + X$ and $p\gamma\text{Pb} \rightarrow J/\psi g\text{Pb} + X$ processes (bottom panels) for the forward detector with ξ (red dashed line), at the CMS-TOTEM forward detector with ξ_1 (green dashed line), at the CMS-TOTEM forward detector with ξ_2 (blue solid line), and at the AFP-ATLAS forward detector with ξ_3 (magenta dash dotted line).

($xG_{g/p}(x, \mu_f)$). While in the γPb ones the photon originates from the proton and the photoproduction cross section is determined by the gluon density of nuclei, which is improved by a factor of the order of $A = 208$ with reference to $xG_{g/p}(x, \mu_f)$. Consequently, the contributions of the γp and γPb interactions are different and the contributions of the γp interactions are larger than those of γPb ones. The experimental disentanglement between the γp and γPb interactions is technically possible by examining the final state by tagging the intact hadron using forward detectors or/and by using the zero-degree calorimeters to veto very forward going neutral fragments. The shapes of the $y^{J/\psi}$ and $\log \xi$ distributions for PbPb collisions in $2 \rightarrow 1$ subprocess are similar and almost symmetric whereas for $2 \rightarrow 2$ subprocess they are totally dissimilar and asymmetric. The dominant $y^{J/\psi}$ and $\log \xi$ distributions also arise from $0.0015 < \xi_2 < 0.5$.

IV. SUMMARY

We examine in this paper the photoproduction of single J/ψ meson to leading order in the NRQCD framework at the LHC with forward detector acceptances. We look into both color-singlet and -octet contributions for different Fock states in pp, PbPb and pPb collision modes. The differential cross sections of $z^{J/\psi}$, $p_T^{J/\psi}$, $y^{J/\psi}$ and $\log \xi$ for J/ψ meson are presented and nuclear shadowing effects are considered. Our results show that the main contribution of the $p_T^{J/\psi}$ distribution comes from the color-octet $^1S_0^{[8]}$ channel. As for $z^{J/\psi}$ distribution, the main contribution arises from the color-singlet $^3S_1^{[1]}$ channel for small- $z^{J/\psi}$ region and $^1S_0^{[8]}$ channel for large- $z^{J/\psi}$ region. The smallest ones are from the $^3S_1^{[8]}$ in the whole range of $z^{J/\psi}$ and $p_T^{J/\psi}$. It has been found that the produced signal relies on the choice of forward detector acceptance, where in our case $0.0015 < \xi_2 < 0.5$ is the one that keeps the largest contribution. The signal PbPb collision is boosted due to the enhancement of the photon flux for nuclei which is proportional to Z^2 , and gluon distribution of lead by a factor of order of A . The large predicted values for the production rates in pp collisions together with in an upgraded pPb collisions indicating that the J/ψ photoproduction should be possible to investigate at the CERN LHC. It may provide more crucial and realistic route toward quarkonium production in inelastic process regime. Its trace at the LHC with forward detector acceptances may be obvious to investigate the color-singlet and color-octet mechanism and will be valuable for exploring the new area of heavy quarkonium production.

Acknowledgments

Tichouk thanks professors Gang Li and Mao Song for very useful discussions. Hao Sun is supported by the National Natural Science Foundation of China (Grant No.11675033) and by the Fundamental Research Funds for the Central Universities (Grant No. DUT18LK27).

Appendix A: LIST OF AMPLITUDE SQUARES

In the appendix, we give the list of the amplitude squares timed long distance matrix elements for the different partonic processes computed with the FORM package [91] of the following states: ${}^3S_1^{[1]}$, ${}^1S_0^{[8]}$, ${}^3S_1^{[8]}$, ${}^3P_0^{[8]}$, ${}^3P_1^{[8]}$, ${}^3P_2^{[8]}$ for the partonic processes $\gamma g \rightarrow Q\bar{Q}[n] + g$ and ${}^1S_0^{[8]}$, ${}^3P_0^{[8]}$, ${}^3P_2^{[8]}$ for $\gamma\gamma \rightarrow Q\bar{Q}[n]$. The amplitude squares timed long distance matrix elements for $2 \rightarrow 2$ partonic processes for different Fock state contributions are

$$\overline{\sum} \left| \mathcal{M} \left[{}^{2S+1}L_J^{[1,8]} \right] \right|^2 = \frac{1}{N_{\text{col}} N_{\text{pol}}} \overline{\sum} |\mathcal{A}_{S,L}|^2 \quad (\text{A1})$$

$$\overline{\sum} \left| \mathcal{M} \left[{}^3S_1^{[1]} \right] \right|^2 = \frac{32(4\pi)^3 \alpha_s^2 e_c^2 ((\hat{s}\hat{t} + \hat{t}\hat{u} + \hat{s}\hat{u})^2 - M_Q^2 \hat{s}\hat{t}\hat{u}) M_{J/\psi}}{27(\hat{s} + \hat{t})^2 (\hat{s} + \hat{u})^2 (\hat{t} + \hat{u})^2} \langle 0 | \mathcal{O}_1^{J/\psi} [{}^3S_1] | 0 \rangle; \quad (\text{A2})$$

$$\overline{\sum} \left| \mathcal{M} \left[{}^1S_0^{[8]} \right] \right|^2 = \frac{3(4\pi)^3 \alpha_s^2 e_c^2 \hat{s}\hat{u} (M_{J/\psi}^8 + \hat{s}^4 + \hat{t}^4 + \hat{u}^4)}{M_{J/\psi} \hat{t} (\hat{s} + \hat{t})^2 (\hat{s} + \hat{u})^2 (\hat{t} + \hat{u})^2} \langle 0 | \mathcal{O}_8^{J/\psi} [{}^1S_0] | 0 \rangle; \quad (\text{A3})$$

$$\overline{\sum} \left| \mathcal{M} \left[{}^3S_1^{[8]} \right] \right|^2 = \frac{20(4\pi)^3 \alpha_s^2 e_c^2 ((\hat{s}\hat{t} + \hat{t}\hat{u} + \hat{s}\hat{u})^2 - M_{J/\psi}^2 \hat{s}\hat{t}\hat{u}) M_{J/\psi}}{9(\hat{s} + \hat{t})^2 (\hat{s} + \hat{u})^2 (\hat{t} + \hat{u})^2} \langle 0 | \mathcal{O}_8^{J/\psi} [{}^3S_1] | 0 \rangle; \quad (\text{A4})$$

$$\begin{aligned} \overline{\sum} \left| \mathcal{M} \left[{}^3P_0^{[8]} \right] \right|^2 &= \frac{4(4\pi)^3 \alpha_s^2 e_c^2}{(\hat{s} + \hat{t})^2 (\hat{s} + \hat{u})^2 (\hat{t} + \hat{u})^2} \left[\frac{9M_{J/\psi}^5 \hat{s}\hat{u}}{\hat{t}} + \frac{\hat{s}\hat{u}\hat{t}^3 (2M_{J/\psi}^4 + 3\hat{t}M_{J/\psi}^2 + \hat{s}\hat{u})^2}{M_{J/\psi}^3 (\hat{s} + \hat{t})^2 (\hat{t} + \hat{u})^2} + \right. \\ &\quad \left. \frac{\hat{s}^3\hat{u} (3\hat{s}^2M_{J/\psi}^2 - \hat{t}\hat{u} (2M_{J/\psi}^2 - \hat{s}))^2}{M_{J/\psi}^3 \hat{t} (\hat{t} + \hat{s})^2 (\hat{s} + \hat{u})^2} + \frac{\hat{u}^3\hat{s} (\hat{s}\hat{t} (2M_{J/\psi}^2 - \hat{u}) - 3\hat{u}^2M_{J/\psi}^2)^2}{M_{J/\psi}^3 \hat{t} (\hat{t} + \hat{s})^2 (\hat{s} + \hat{u})^2} \right] \langle 0 | \mathcal{O}_8^{J/\psi} [{}^3P_0] | 0 \rangle; \end{aligned} \quad (\text{A5})$$

$$\begin{aligned} \overline{\sum} \left| \mathcal{M} \left[{}^3P_1^{[8]} \right] \right|^2 &= \frac{8(4\pi)^3 \alpha_s^2 e_c^2}{M_{J/\psi}^3 (\hat{s} + \hat{t})^4 (\hat{s} + \hat{u})^4 (\hat{t} + \hat{u})^4} [\hat{s}^7 (\hat{t}^4 + 2\hat{t}^3\hat{u} + 4\hat{t}^2\hat{u}^2 + 2\hat{t}\hat{u}^3 + \hat{u}^4) + \hat{s}^6 (\hat{t} + \hat{u})^2 \\ &\quad \times (3\hat{t}^3 + 7\hat{t}^2\hat{u} + 7\hat{t}\hat{u}^2 - \hat{u}^3) + \hat{s}^5 (3\hat{t}^6 + 22\hat{t}^5\hat{u} + 60\hat{t}^4\hat{u}^2 + 76\hat{t}^3\hat{u}^3 + 36\hat{t}^2\hat{u}^4 + \\ &\quad 4\hat{t}\hat{u}^5 - \hat{u}^6) + \hat{s}^4 (\hat{t} + \hat{u}) (\hat{t}^6 + 12\hat{t}^5\hat{u} + 46\hat{t}^4\hat{u}^2 + 72\hat{t}^3\hat{u}^3 + 32\hat{t}^2\hat{u}^4 + 4\hat{t}\hat{u}^5 + \\ &\quad \hat{u}^6) + 2\hat{s}^3\hat{t}\hat{u} (\hat{t}^6 + 10\hat{t}^5\hat{u} + 38\hat{t}^4\hat{u}^2 + 59\hat{t}^3\hat{u}^3 + 38\hat{t}^2\hat{u}^4 + 10\hat{t}\hat{u}^5 + \hat{u}^6) + \\ &\quad 2\hat{s}^2\hat{t}^2\hat{u}^2 (\hat{t} + \hat{u}) (\hat{t}^4 + 9\hat{t}^3\hat{u} + 20\hat{t}^2\hat{u}^2 + 10\hat{t}\hat{u}^3 + 2\hat{u}^4) + \hat{s}\hat{t}^3\hat{u}^3 (\hat{t} + \hat{u})^2 \\ &\quad \times (2\hat{t}^2 + 9\hat{t}\hat{u} + 2\hat{u}^2) + \hat{t}^4\hat{u}^4 (\hat{t} + \hat{u})^3] \langle 0 | \mathcal{O}_8^{J/\psi} [{}^3P_1] | 0 \rangle; \end{aligned} \quad (\text{A6})$$

$$\begin{aligned} \overline{\sum} \left| \mathcal{M} \left[{}^3P_2^{[8]} \right] \right|^2 &= \frac{8(4\pi)^3 \alpha_s^2 e_c^2}{5M_{J/\psi}^3 \hat{t} (\hat{s} + \hat{t})^4 (\hat{s} + \hat{u})^4 (\hat{t} + \hat{u})^4} [12\hat{s}^9\hat{u} (\hat{t} + \hat{u})^2 + 12\hat{s}^8\hat{u} (\hat{t} + \hat{u}) (5\hat{t}^2 + \\ &\quad 7\hat{t}\hat{u} + 4\hat{u}^2) + \hat{s}^7 (3\hat{t}^5 + 142\hat{t}^4\hat{u} + 384\hat{t}^3\hat{u}^2 + 454\hat{t}^2\hat{u}^3 + 303\hat{t}\hat{u}^4 + 96\hat{u}^5) + \\ &\quad \hat{s}^6 (\hat{t} + \hat{u}) (9\hat{t}^5 + 202\hat{t}^4\hat{u} + 438\hat{t}^3\hat{u}^2 + 442\hat{t}^2\hat{u}^3 + 309\hat{t}\hat{u}^4 + 120\hat{u}^5) + \\ &\quad \hat{s}^5 (9\hat{t}^7 + 198\hat{t}^6\hat{u} + 736\hat{t}^5\hat{u}^2 + 1200\hat{t}^4\hat{u}^3 + 1184\hat{t}^3\hat{u}^4 + 860\hat{t}^2\hat{u}^5 + \\ &\quad 429\hat{t}\hat{u}^6 + 96\hat{u}^7) + \hat{s}^4 (\hat{t} + \hat{u}) (3\hat{t}^7 + 100\hat{t}^6\hat{u} + 450\hat{t}^5\hat{u}^2 + 720\hat{t}^4\hat{u}^3 + \\ &\quad 688\hat{t}^3\hat{u}^4 + 496\hat{t}^2\hat{u}^5 + 255\hat{t}\hat{u}^6 + 48\hat{u}^7) + 2\hat{s}^3\hat{u} (11\hat{t}^8 + 114\hat{t}^7\hat{u} + \\ &\quad 362\hat{t}^6\hat{u}^2 + 585\hat{t}^5\hat{u}^3 + 600\hat{t}^4\hat{u}^4 + 440\hat{t}^3\hat{u}^5 + 227\hat{t}^2\hat{u}^6 + 66\hat{t}\hat{u}^7 + \\ &\quad 6\hat{u}^8) + 2\hat{s}^2\hat{t}\hat{u}^2 (\hat{t} + \hat{u})^2 (19\hat{t}^5 + 76\hat{t}^4\hat{u} + 104\hat{t}^3\hat{u}^2 + 84\hat{t}^2\hat{u}^3 + \\ &\quad 48\hat{t}\hat{u}^4 + 12\hat{u}^5) + \hat{s}\hat{t}^2\hat{u}^3 (\hat{t} + \hat{u})^2 (22\hat{t}^4 + 59\hat{t}^3\hat{u} + \\ &\quad 58\hat{t}^2\hat{u}^2 + 36\hat{t}\hat{u}^3 + 12\hat{u}^4) + 3(\hat{t} + \hat{u})^3 \hat{t}^5\hat{u}^4] \langle 0 | \mathcal{O}_8^{J/\psi} [{}^3P_2] | 0 \rangle. \end{aligned} \quad (\text{A7})$$

The amplitude squares timed long distance matrix elements for $2 \rightarrow 1$ partonic processes for different Fock state contributions are

$$\overline{\sum} \left| \mathcal{M} \left[{}^1S_0^{[8]} \right] \right|^2 = \frac{(4\pi)^2 \alpha_s e_c^2}{2M_{J/\psi}} \langle 0 | \mathcal{O}_8^{J/\psi} [{}^1S_0] | 0 \rangle; \quad (\text{A8})$$

$$\overline{\sum} \left| \mathcal{M} \left[{}^3P_0^{[8]} \right] \right|^2 = \frac{6(4\pi)^2 \alpha_s e_c^2}{M_{J/\psi}^3} \langle 0 | \mathcal{O}_8^{J/\psi} [{}^3P_0] | 0 \rangle; \quad (\text{A9})$$

$$\overline{\sum} \left| \mathcal{M} \left[{}^3P_2^{[8]} \right] \right|^2 = \frac{8(4\pi)^2 \alpha_s e_c^2}{5M_{J/\psi}^3} \langle 0 | \mathcal{O}_8^{J/\psi} [{}^3P_2] | 0 \rangle. \quad (\text{A10})$$

-
- [1] G. T. Bodwin, E. Braaten, and G. P. Lepage, *Rigorous QCD analysis of inclusive annihilation and production of heavy quarkonium*, Phys. Rev. D 51 (1995) 1125; Erratum: Phys. Rev. D 55 (1997) 5853, [[arXiv:hep-ph/9407339](#)].
- [2] G. A. Schuler, *Quarkonium production: Velocity scaling rules and long distance matrix elements*, Int. J. Mod. Phys. A 12 (1997) 3951, [[arXiv:hep-ph/9702230](#)].
- [3] A. Gerhard, and Schuler, *Quarkonium production: Velocity scaling rules and long distance matrix elements*, Int. J. Mod. Phys. A 12 (1997) 3951, [[arXiv:hep-ph/9702230](#)].
- [4] B. A. Kniehl and C. P. Palisoc, *Prompt J/ψ plus photon associated electroproduction at DESY HERA*, Eur. Phys. J. C 48 (2006) 451, [[arXiv:hep-ph/0608245](#)].
- [5] K.-T. Chao and L.-K. Hao, *Charmonium production in e^+e^- annihilation at $\sqrt{s} = 10.6\text{-GeV}$* , Nucl. Phys. Proc. Suppl. 115 (2003) 162, [[arXiv:hep-ph/0209189](#)].
- [6] J. Soto, *Overview of charmonium decays and production from Non-Relativistic QCD*, Int. J. Mod. Phys. Conf. Ser. 02 (2011) 1, [[arXiv:1101.2392](#)].
- [7] Z. Sun, X.-G. Wu, and H.-F. Zhang, *Prompt J/ψ production in association with a $c\bar{c}$ pair within the framework of nonrelativistic QCD via photon-photon collisions at the International Linear Collider*, Phys. Rev. D 92 (2015) 074021, [[arXiv:1507.08190](#)].
- [8] G. C. Nayak, *Proof of NRQCD factorization at all orders in the coupling constant in heavy quarkonium production*, Eur. Phys. J. C 76 (2016) 448, [[arXiv:1506.02593](#)].
- [9] R. Barbieri, M. Caffo, R. Gatto, and E. Remiddi, *QCD corrections to P wave quarkonium decays*, Nucl. Phys. B 192 (1981) 61.
- [10] F. Abe et al., *J/ψ and $\psi(2S)$ Production in $p\bar{p}$ Collisions at $\sqrt{s}=1.8\text{TeV}$* , Phys. Rev. Lett. 79 (1997) 572.
- [11] N. Brambilla et al., *Heavy quarkonium: progress, puzzles, and opportunities*, Eur. Phys. J. C 71 (2011) 1534, [[arXiv:1010.5827](#)].
- [12] Z.-G. He and J.-X. Wang, *Inclusive J/ψ production in Υ decay via color-singlet mechanism*, Phys. Rev. D 81 (2010) 054030, [[arXiv:0911.0139](#)].
- [13] Z. Sun and H.-F. Zhang, *QCD corrections to the color-singlet J/ψ production in deeply inelastic scattering at HERA*, Phys. Rev. D 96 (2017) 091502, [[arXiv:1705.05337](#)].
- [14] C. E. Carlson and R. Suaya, *Hadronic production of the ψ/J meson*, Phys. Rev. D 14 (1976) 3115.
- [15] G. C. Nayak, *Correct definition of color singlet P-wave non-perturbative matrix element of heavy quarkonium production*, JHEP 1709 (2017) 090, [[arXiv:1704.07449](#)].
- [16] M. B. Einhorn and S. D. Ellis, *Hadronic production of the new resonances: Probing gluon distributions*, Phys. Rev. D 12 (1975) 2007.
- [17] E. L. Berger and D. Jones, *Inelastic photoproduction of J/ψ and Υ by gluons*, Phys. Rev. D 23 (1981) 1521.
- [18] Z.-G. He and J.-X. Wang, *Color-singlet J/ψ production at $\mathcal{O}(\alpha_s^6)$ in Υ decay*, Phys. Rev. D 82 (2010) 094033, [[arXiv:1009.1563](#)].
- [19] R. Baier and R. Rckl, *Hadronic production of J/ψ and Υ : Transverse momentum distributions*, Phys. Lett. B 102 (1981) 364.
- [20] R. Baier and R. Rckl, *On inelastic leptonproduction of heavy quarkonium states*, Nucl. Phys. B 201 (1982) 1.
- [21] G. T. Bodwin, H. S. Chung, D. Kang, J. Lee, and C. Yu, *Improved determination of color-singlet nonrelativistic QCD matrix elements for S-wave charmonium*, Phys. Rev. D 77 (2008) 094017, [[arXiv:0710.0994](#)].
- [22] S. D. Ellis, M. B. Einhorn, and C. Quigg, *Comment on Hadronic Production of Psions*, Phys. Rev. Lett. 36 (1976) 1263.
- [23] C. Chao-Hsi, *Hadronic production of J/ψ associated with a gluon*, Nucl. Phys. B 172 (1980) 425.
- [24] M. Klasen, Kniehl, A. Bernd, L. N. Mihaila, and M. Steinhauser, *Evidence for color octet mechanism from CERN LEP-2 $\gamma\gamma \rightarrow J/\psi + X$ data*, Phys. Rev. Lett. 89 (2002) 032001, [[arXiv:hep-ph/0112259](#)].
- [25] G. T. Bodwin, E. Braaten, and J. Lee, *Comparison of the color-evaporation model and the NRQCD factorization approach in charmonium production*, Phys. Rev. D 72 (2005) 014004, [[arXiv:hep-ph/0504014](#)].

- [26] F. G. Ben, M. V. T. Machado, and W. K. Sauter, *Polarization of prompt J/ψ and $\Upsilon(1S)$ production in the color evaporation model*, Phys. Rev. D 96 (2017) 054014, [arXiv:1706.07686].
- [27] Y.-Q. Ma and R. Vogt, *Quarkonium production in an improved color evaporation model*, Phys. Rev. D 94 (2016) 114029, [arXiv:1609.06042].
- [28] D. Kang, J.-W. Lee, J. Lee, T. Kim, and P. Ko, *Color-evaporation-model calculation of $e^+e^- \rightarrow J/\psi + c\bar{c} + X$ at $\sqrt{s} = 10.6\text{GeV}$* , Phys. Rev. D 71 (2005) 094019, [arXiv:hep-ph/0412381].
- [29] B. A. Kniehl and G. Kramer, *Charmonium production via fragmentation at DESY HERA*, Phys. Rev. D 56 (1997) 5820, [arXiv:hep-ph/9706369].
- [30] Y.-Q. Ma, J.-W. Qiu, and H. Zhang, *Heavy quarkonium fragmentation functions from a heavy quark pair. II. P wave*, Phys. Rev. D 89 (2014) 094030, [arXiv:1401.0524]; *Heavy quarkonium fragmentation functions from a heavy quark pair. I. S wave*, Phys. Rev. D 89 (2014) 094029, [arXiv:1311.7078].
- [31] F. Yuan, H.-S. Dong, L.-K. Hao, and K.-T. Chao, *Inelastic J/ψ production in polarized photon-hadron collisions*, Phys. Rev. D 61 (2000) 114013, [arXiv:hep-ph/9909221].
- [32] M. Cacciari and M. Kramer, Michael, *Color-Octet Contributions to J/ψ Photoproduction*, Phys. Rev. Lett. 76 (1996) 4128, [arXiv:hep-ph/9601276].
- [33] J. Amundson, S. Fleming, and I. Maksymyk, *Photoproduction of J/ψ in the forward region*, Phys. Rev. D 56 (1997) 5844, [arXiv:hep-ph/9601298].
- [34] P. Ko, J. Lee, and H. S. Song, *Color-octet mechanism in $\gamma + p \rightarrow J/\psi + X$* , Phys. Rev. D 54 (1996) 4312, [Erratum: Phys. Rev. D 60 (1999) 119902], [arXiv:hep-ph/9602223].
- [35] G. Chen, X.-G. Wu, Z. Sun, S.-Q. Wang, and J.-M. Shen, *Exclusive charmonium production from e^+e^- annihilation round the Z^0 peak*, Phys. Rev. D 88 (2013) 074021, [arXiv:1308.5375].
- [36] H. Pereira Da Costa (ALICE), *Charmonium production in pp collisions with ALICE at the LHC*, J. Phys. Conf. Ser. 779 (2017) 012036, [arXiv:1609.07277].
- [37] M. Krmer, *Quarkonium production at high-energy colliders*, Prog. Part. Nucl. Phys. 47 (2001) 141, [arXiv:hep-ph/0106120].
- [38] M. G Albrow et al., *The FP420 R&D project: Higgs and New Physics with forward protons at the LHC*, JINST 4 (2009) T10001, [arXiv:0806.0302].
- [39] R. Staszewski, *The AFP Project*, Acta Phys. Polon. B 42 (2011) 1615, [arXiv:1104.1858].
- [40] H. Sun, *Probing the diffractive production of a Z-boson pair at forward rapidities at the LHC*, Phys. Rev. D 95 (2017) 056023, [arXiv:1703.02692].
- [41] H. Sun, *Large extra dimension effects through light-by-light scattering at the CERN LHC*, Eur. Phys. J. C 74 (2014) 2977, [arXiv:1406.3897].
- [42] M. Köksal and S. C. Inan, *Anomalous $tq\gamma$ Couplings in γp Collision at the LHC*, Adv. High Energy Phys. 2014 (2014) 935840, [arXiv:1305.7096].
- [43] O. Kepka, and C. Royon, *Anomalous $WW\gamma$ coupling in photon-induced processes using forward detectors at the CERN LHC*, Phys. Rev. D 78 (2008) 073005, [arXiv:0808.0322].
- [44] E. Chapon, C. Royon, and O. Kepka, *Anomalous quartic $WW\gamma\gamma$, $ZZ\gamma\gamma$, and trilinear $WW\gamma$ couplings in two-photon processes at high luminosity at the LHC*, Phys. Rev. D 81 (2010) 074003, [arXiv:0912.5161].
- [45] M. I. Vysotsky and E. Zhemchugov, *Equivalent photons in proton-proton and ion-ion collisions at the LHC*, (2018) 10.3367/UFNe.2018.07.038389, [arXiv:1806.07238].
- [46] S. T. Monfared, S. Fayazbakhsh, and M. M. Najafabadi, *Exploring anomalous $HZ\gamma$ couplings in γ -proton collisions at the LHC*, Phys. Lett. B 762 (2016) 301, [arXiv: hep-ph/1610.02883].
- [47] B. Sahin and Billur, A. A. Billur, *Anomalous Wtb couplings in γp collision at the LHC*, Phys. Rev. D 86 (2012) 074026, [arXiv:1210.3235].
- [48] G. -C. Cho, T. Kono, K. Mawatari, and K. Yamashita, *Search for Kaluza-Klein gravitons in extra dimension models via forward detectors at the LHC*, Phys. Rev. D 91 (2015) 115015, [arXiv:1503.05678].
- [49] H. Sun, *Dark matter searches in jet plus missing energy events in γp collisions at the CERN LHC*, Phys. Rev. D 90 (2014) 035018, [arXiv:1407.5356].
- [50] H. Sun, W. Liu, X.-J. Wang, Y.-J. Zhou, and H.-S. Hou, *NLO QCD corrections to Single Top and W associated photoproduction at the LHC with forward detector acceptances*, JHEP 1502 (2015) 064, [arXiv:1408.1218].
- [51] B. E. Cox, F. K. Loebinger, and A. D. Pilkington, *Detecting Higgs bosons in the $b\bar{b}$ decay channel using forward proton tagging at the LHC*, JHEP 10 (2007) 090, [arXiv:0709.3035].
- [52] C. Royon, *The ATLAS Forward Physics Project*, [arXiv:1302.0623].
- [53] C. Royon, *Forward physics with proton tagging at the LHC*, J. Phys. Conf. Ser. 455 (2013) 012055, [arXiv:1305.0652].
- [54] M. Chaichian, P. Hoyer, K. Huitu, V. A. Khoze, and A. D. Pilkington, *Searching for the triplet Higgs sector via central exclusive production at the LHC*, JHEP 05 (2009) 011, [arXiv:0901.3746].
- [55] C. Royon and N. Cartiglia, *The AFP and CT-PPS projects*, Int. J. Mod. Phys. A 29 (2014) 1446017, [arXiv:1503.04632].
- [56] C. Royon, *The ATLAS Forward Physics Program*, PoS DIS2010 (2010) 088, [arXiv:1008.3207].
- [57] R. Staszewski, J. Chwastowski, K. Korcyl, and M. Trzebinski, *Alignment-related Effects in Forward Proton Experiments at the LHC*, Nucl. Instrum. Meth. A801 (2015) 34, [arXiv:1412.0946].
- [58] V. Khachatryan et. al. (CMS), *Measurement of diffraction dissociation cross sections in pp collisions at $\sqrt{s} = 7\text{TeV}$* , Phys. Rev. D92 (2015) 012003, [arXiv:1503.08689].
- [59] E. Nurse and S. Sen, *Methods to Select Soft Diffraction Dissociation at the LHC*, Adv. High Energy Phys. 2016 (2016) 5082847, [arXiv:1107.2688].

- [60] B. E. Cox, *A Review of forward proton tagging at 420m at the LHC, and relevant results from the Tevatron and HERA*, AIP Conf. Proc. 753 (2005) 103, [arXiv:hep-ph/0409144].
- [61] D. d'Enterria, *Forward Physics at the LHC: within and beyond the Standard Model*, AIP Conf. Proc. 1038 (2008) 95, [arXiv:0806.0883].
- [62] K. Akiba et al., *LHC Forward Physics*, J. Phys. G 43 (2016) 110201, [arXiv:1611.05079].
- [63] N. Armesto, *Nuclear shadowing*, J. Phys. G 32 (2006) R367, [arXiv:hep-ph/0604108].
- [64] K. J. Eskola, H. Paukkunen, and C. A. Salgado, *EPS09: A New Generation of NLO and LO Nuclear Parton Distribution Functions*, JHEP 04, 065 (2009), [arXiv:0902.4154].
- [65] U. D. Jentschura and V. G. Serbo, *Nuclear form factor, validity of the equivalent photon approximation and Coulomb corrections to muon pair production in photon-nucleus and nucleus-nucleus collisions*, Eur. Phys. J. C64 (2009) 309, [arXiv:0908.3853].
- [66] M. Alvioli, C. Ciofi degli Atti, B. Z. Kopeliovich, I. K. Potashnikova, and I. Schmidt, *Diffraction on Nuclei: Effects of Nucleon Correlations*, Phys. Rev. C81, 025204 (2010), [arXiv:0911.1382].
- [67] L.V. Gribov, E.M. Levin and M.G. Ryskin, *Singlet Structure Function at Small x: Unitarization of Gluon Ladders*, Nucl. Phys. B188 (1981) 555; *Semihard Processes in QCD*, Phys. Rep. 100 (1983) 1.
- [68] A. Petrelli, M. Cacciari, M. Greco, F. Maltoni, and M. L. Mangano, *NLO production and decay of quarkonium*, Nucl. Phys. B 514 (1998) 245.
- [69] J. Pumplin, D. R. Stump, J. Huston, H.-L. Lai, P. Nadolsky, and W.-K. Tung, *New Generation of Parton Distributions with Uncertainties from Global QCD Analysis*, JHEP 0207 (2002) 012, [arXiv:0201195].
- [70] V. P. Goncalves and M. M. Machado, *Inelastic quarkonium photoproduction in hadron-hadron interactions at LHC energies*, Eur. Phys. J. A50 (2014) 72, [arXiv:1309.0664].
- [71] K.-T. Chao, Y.-Q. Ma, H.-S. Shao, K. Wang, and Y.-J. Zhang, *J/ψ Polarization at Hadron Colliders in Nonrelativistic QCD*, Phys. Rev. Lett. 108 (2012) 242004, [arXiv:1201.2675].
- [72] A. G. Ståhl (CMS), *Charmonium production in pp, pPb and PbPb collisions with CMS*, J. Phys. Conf. Ser. 832 (2017) 012031.
- [73] A. Andronic et al., *Heavy-flavour and quarkonium production in the LHC era: from proton-proton to heavy-ion collisions*, Eur. Phys. J. C76, 107 (2016), [arXiv:1506.03981 [nucl-ex]].
- [74] S. Peigne and A. Peshier, *Collisional energy loss of a fast heavy quark in a quark-gluon plasma*, Phys. Rev. D77 (2008) 114017, [arXiv:0802.4364 [hep-ph]].
- [75] V. P. Goncalves, *Photoproduction of top quarks in coherent hadron-hadron interactions*, Phys. Rev. D 88 (2013) 054025.
- [76] D. d'Enterria and J.-P. Lansberg, *Study of Higgs boson production and its $b\bar{b}$ decay in $\gamma - \gamma$ processes in proton-nucleus collisions at the LHC*, Phys. Rev. D 81 (2010) 014004, [arXiv:0909.3047].
- [77] M. Butenschoen and B. A. Kniehl, *Complete next-to-leading-order corrections to J/ψ photoproduction in nonrelativistic quantum chromodynamics*, Phys. Rev. Lett. 104 (2010) 072001, [arXiv:0909.2798].
- [78] E. Braaten, M. A. Doncheski, S. Fleming, and M. L. Mangano, *Fragmentation production of J/ψ and ψ' at the Tevatron*, Physics Letters B 333 (1994) 548, [arXiv:hep-ph/9405407].
- [79] S. Rajesh, R. Kishore, and A. Mukherjee, *Sivers effect in Inelastic J/ψ Photoproduction in ep^\dagger Collision in Color Octet Model*, Phys. Rev. D 98 (2018) 014007, [arXiv:1802.10359].
- [80] B. Paul, M. Mandal, P. Roy, and S. Chattapadhyay, *Systematic study of charmonium production in pp collisions at LHC energies*, J. Phys. G42 (2015) 065101, [arXiv:1411.6783 [hep-ph]].
- [81] V. Khachatryan et al. (CMS), *Prompt and non-prompt J/ψ production in pp collisions at $\sqrt{s} = 7$ TeV*, Eur. Phys. J. C71, 1575 (2011), [arXiv:1011.4193 [hep-ex]].
- [82] L. A. Linden Levy, *From production to suppression, a critical review of charmonium measurements at RHIC*, Nucl. Phys. A 830 (2009) 353C, [arXiv:0908.2361 [nucl-ex]].
- [83] B. A. Kniehl and G. Kramer, *TEVATRON - HERA color - octet charmonium anomaly versus higher order QCD effects*, Eur. Phys. J. C 6 (1999) 493, [arXiv:hep-ph/9803256].
- [84] M. Klasen, T. Kleinwort, and G. Kramer, *Inclusive Jet Production in γp and $\gamma\gamma$ Processes: Direct and Resolved Photon Cross Sections in Next-To-Leading Order QCD*, Eur. Phys. J. direct 1(1998) 1, [arXiv:hep-ph/9712256].
- [85] R. M. Godbole, D. Indumathi, and M. Kramer, *J/ψ production through resolved photon processes at e^+e^- colliders*, Phys. Rev. D 65 (2002) 074003, [arXiv:hep-ph/0101333].
- [86] F. D. Aaron et al. [H1 Collaboration], *Inelastic Production of J/ψ Mesons in Photoproduction and Deep Inelastic Scattering at HERA*, Eur. Phys. J. C 68, 401 (2010), [arXiv:1002.0234].
- [87] S. Chekanov et al. (ZEUS), *Measurements of inelastic J/ψ and ψ' photoproduction at HERA*, Eur. Phys. J. C27 (2003) 173, [arXiv:hep-ex/0211011].
- [88] P. Artoisenet, J. M. Campbell, F. Maltoni, and F. Tramontano, *J/ψ production at HERA*, Phys. Rev. Lett. 102 (2009) 142001, [arXiv:0901.4352].
- [89] M. Kramer, *QCD corrections to inelastic J/ψ photoproduction*, Nucl. Phys. B 459, 3 (1996).
- [90] M. Kramer, J. Zunft, J. Steegborn and P. M. Zerwas, *Inelastic J/ψ photoproduction*, Phys. Lett. B 348, 657 (1995), [arXiv:hep-ph/9411372].
- [91] J. Kuipers, T. Ueda, J. Vermaseren, and J. Vollinga, *FORM version 4.0*, Comput. Phys. Commun 184 (2013) 1453, [arXiv:1203.6543].